Applied Physics Letters ARTICLE scitation.org/journal/apl

Determining the temperature-dependent London penetration depth in HTS thin films and its effect on SQUID performance

Cite as: Appl. Phys. Lett. **119**, 142601 (2021); doi: 10.1063/5.0065790
Submitted: 5 August 2021 · Accepted: 17 September 2021 ·
Published Online: 5 October 2021

View Online Export Citation CrossMark

Shane Keenan,[1,a)] Colin Pegrum,[2,a)] Marc Gali Labarias,[1] and Emma E. Mitchell[1]

AFFILIATIONS

[1]CSIRO Manufacturing, West Lindfield, New South Wales 2070, Australia
[2]Department of Physics, University of Strathclyde, Glasgow G4 0NG, United Kingdom

[a)]Authors to whom correspondence should be addressed: shane.keenan@csiro.au and colin.pegrum@strath.ac.uk

ABSTRACT

The optimum design of high-sensitivity Superconducting Quantum Interference Devices (SQUIDs) and other devices based on thin high-temperature superconductor (HTS) films requires accurate inductance modeling. This needs the London penetration depth λ to be well defined, not only at 77 K, but also for any operating temperature, given the increasingly widespread use of miniature low-noise single-stage cryocoolers. Temperature significantly affects all inductances in any active superconducting device, and cooling below 77 K can greatly improve device performance; however, accurate data for the temperature dependence of inductance and $\lambda(T)$ for HTS devices are largely missing in the literature. We report here inductance measurements on a set of 20 different thin-film $YBa_2Cu_3O_{7-x}$ SQUIDs at 77 K with thickness $t = 220$ or 113 nm. By combining experimental data and inductance modeling, we find an average penetration depth $\lambda(77) = 391$ nm at 77 K, which was independent of t. Using the same methods, we derive an empirical expression for $\lambda(T)$ for a further three SQUIDs measured on a cryocooler from 50 to 79 K. Our measured value of $\lambda(77)$ and our inductance extraction procedures were then used to estimate the inductances and the effective areas of directly coupled SQUID magnetometers with large washer-style pickup loops. The latter agrees better than 7% with experimentally measured values, validating our measured value of $\lambda(77)$ and our inductance extraction methods.

SQUIDs are the most sensitive magnetic field detectors with a wide range of proven applications outside the laboratory,[1–3] such as airborne,[4] ground,[5] and marine[6] surveying, archaeology[7] or nondestructive evaluation.[8] High-temperature superconductor (HTS) SQUIDs made from $YBa_2Cu_3O_{7-x}$ (YBCO) are especially attractive for such uses, as they can be used in liquid nitrogen at 77 K and also in compact single-stage cryocoolers, where cooling below 77 K can enhance their performance significantly.

For thin-film SQUIDs and related devices, the inductances of all their parts need to be known at the design stage in order to optimize performance at a given temperature T. These inductances depend significantly on T due to the changing penetration depth $\lambda(T)$, especially approaching the transition temperature T_c, as our data reported here will show. There are very few recent measurements of λ similar to ours on high-quality YBCO films. This motivated us to make direct inductance measurements on a set of YBCO SQUIDs with different linewidths, loop sizes, and film thicknesses and to combine these with inductance extraction techniques to find the penetration depth $\lambda(77)$ at 77 K and also an expression for $\lambda(T)$ in the range $50 < T < 78$ K.

Design can be supported by various inductance extraction tools or formulas available for self-inductance, but whatever the method, these all need $\lambda(T)$ as a parameter. For example, the inductance L_{sq} of a SQUID must be well known to optimize the modulation parameter $\beta_L = 2L_{sq}I_c/\Phi_0$ (I_c is the junction critical current, and Φ_0 is the flux quantum). This is also true for the loops in Superconducting Quantum Interference Filters (SQIFs).[9] SQIFs have a large dynamic range[10] that makes them well-suited to operation below 77 K in a cryocooler, and their loop inductances need to be known for the chosen operating temperature. Inductances of the component parts of direct-coupled SQUID magnetometers[11] also need to be known accurately to determine their effective area.

One way to measure λ in HTS thin films is the two-coil mutual inductance technique first developed by Fiory *et al.*[12] or variations on this.[13–15] More advanced techniques include muon spin rotation and

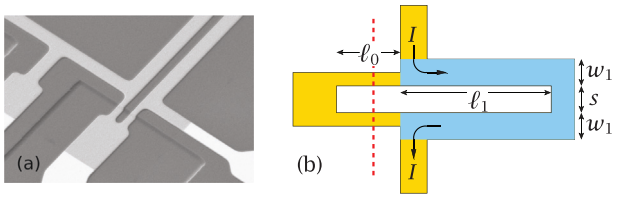

FIG. 1. (a) SEM of part of a SQUID with step-edge junctions 2 μm wide. (b) The SQUID model. Injected current I flows through the CPS part, shown in blue. The red dashed line indicates the step edge.

microwave resonance.[15,16] All these are limited to large millimeter-sized samples. Our approach is to deduce $\lambda(T)$ from direct measurements of inductance in SQUIDs, like those in Fig. 1.

These all have a co-planar strip line (CPS) design, shorted at one end, with 2 μm wide step-edge junctions. This is the design used in our directly coupled magnetometers,[11] which we discuss later. We measure the coupled self inductance L_{co} of the part of the SQUID loop shown in blue in Fig. 1(b), which has length ℓ_1. An external current I is fed through this. (In our magnetometers, this would be the current sensed by the directly coupled pickup loop, which is absent for these measurements.) The total SQUID inductance $L_{sq} = L_{co} + L_{par}$, where L_{par} is the parasitic inductance of the uncoupled part with length ℓ_0. From the change δI causing an output change of one flux quantum Φ_0, $L_{co} = \Phi_0/\delta I$. A technique like this was used for HTS SQUIDs by Forrester *et al.*[17] and subsequently by others.[18–24]

Measurements similar to ours have been made by several others on SQUIDs to find λ. Li *et al.*[21] measured L_{sq} for five nano-slit SQUIDs fabricated by a focused helium ion beam on a 25 nm thick YBCO film and found $\lambda = 180$ nm gave the best match to experiment at 9 K. Ruffieux *et al.*[22,23] measured the inductance of ten HTS SQUIDs fabricated from two separate 140 nm thick YBCO films on $SrTiO_3$ substrates, one with a CeO_2 buffer layer and one without, with varying ℓ_1. They reported λ in the ranges 542–648 nm for no CeO_2 and 313–426 nm with CeO_2. They saw large differences in λ between SQUIDs on the same sample, which they attributed to differences in film thickness and T_c across the sample and slight temperature variation during measurements. Mitchell *et al.*[20] made earlier inductance measurements on seven different CPS SQUIDs made from 300 nm YBCO films and found the inductance per unit length $L_0 = 0.97$ pH/μm for $w_1 = 2$ μm and $s = 4$ μm.

Our present work was done in three related parts. First, we measured L_{co} for twenty bare SQUIDs of different geometries at 77 K (with no magnetometer loop attached) and used inductance extraction models to determine $\lambda(77)$. The SQUID properties are listed in Table I; they are in five sets with different properties, and for each set, ℓ_1 has four different values. For each set, we measured $L_{co}(\ell_1)$ and derived the inductance per unit length L_0 of the CPS by linear regression. We combined our experimental measurements of L_0 with inductance extraction data from SQUID models in which λ is a variable parameter, to find $\lambda(77)$ for the five different samples.

In the second part, we measured $L_{co}(T)$ in a cryocooler for three different SQUIDs on one chip, to extract an empirical expression for $\lambda(T)$. We measured $L_{co}(T)$ for each, for $50 < T < 78$ K. By inductance extraction, we found an expression for $L_{co}(\lambda)$, merged this with the experimental $L_{co}(T)$ and fitted these data to get an expression for $\lambda(T)$.

In the concluding part, we used our value of $\lambda(77)$ and our inductance extraction techniques to estimate the effective area of washer-coupled SQUID magnetometers and compared these with measured effective areas.

L_{co} depends on device structure and film properties and has three contributions, from internal and external magnetic energy, L_m and L_{ext}, respectively, plus a kinetic contribution L_{kin}. In general, $L_{kin} \gg L_m$. Both L_m and L_{kin} depend on λ; as λ increases, L_{kin} diverges rapidly, whereas L_{ext} reaches a limiting value as field penetration nears completion. For a single isolated line, L_{kin} is approximately $(\mu_0\lambda^2)/wt$ per unit length,[25] where μ_0 is the magnetic permeability and w and t are its width and thickness. For the lines in the CPS we use, especially ones with a narrow spacing s, L_{kin} differs somewhat from this expression.[26] We chose to determine inductances using the extraction package `3D-MLSI`,[27,28] rather than from formulas, which may have limited accuracy for our designs. `3D-MLSI` is a Finite Element Method (FEM) and can handle thin-film structures of any arbitrary geometry. It extracts the total inductance $L_{kin} + L_m + L_{ext}$.

Our SQUIDs were fabricated from 113 and 220 nm of YBCO on one side of polished 1 cm^2 MgO substrates using step-edge junctions.[29,30] The films were deposited by Ceraco Ceramic Coating GmbH[31] by reactive co-evaporation, who measured the T_c values listed in Table I inductively[12,13] on unpatterned samples. We have also made resistance-temperature measurements on 4 μm tracks within patterned devices and find that post-deposition processing causes negligible reduction in T_c. All films of both thicknesses have a similar current density, $J_c = 3.1$–3.2 MA/cm^2. Devices were patterned and etched by our standard photo-lithography procedure.[29] We have reported previously current–voltage characteristics of our junctions at

TABLE I. Summary of the film thickness t, T_c, and dimensions of twenty SQUIDs in five sets used in the first part of this study. They are on three separate substrates S1, S2, and S3 and from three different film batches B1, B2, and B3. Each set has four different values of ℓ_1. All have the layout shown in Fig. 1 with $\ell_0 = 10$ μm.

SQUID set	S1-A	S2-A	S3-A	S3-B	S3-C
Batch	B1	B2	B3	B3	B3
T_c (K)	85.9	86.2	87.5	87.5	87.5
t (nm)	220	113	113	113	113
s (μm)	4	4	4	4	2
w_1 (μm)	4	4	4	8	8
ℓ_1 (μm)	{50, 75, 100, 125	20, 34, 44, 50	20, 34, 44, 50	20, 30, 40, 50	20, 30, 40, 50}

77 K (Ref. 30) and typical voltage–flux responses for SQUIDs using them.[11]

In the first part of our work, we measured L_{co} for the 20 SQUIDs in liquid nitrogen inside six concentric mu-metal shields, using a STAR Cryoelectronics PCI-1000 control unit.[32] The encapsulated chip was mounted on a radio frequency shielded probe. Each SQUID was current biased to its optimal operating point (maximum peak to peak voltage modulation) and flux varied by the current I. The PCI-1000 12-bit high-resolution internal current generator supplied I, which was averaged over a minimum of 10 Φ_0 to improve accuracy. We used a 5 Hz triangle waveform for this and a transfer coefficient of 10 μA/V. The amplitude was then varied to couple 10 Φ_0 or more into the SQUID. The PCI-1000 user manual has full details.[32]

Figure 2 plots the experimental L_{co} as a function of ℓ_1 for each of the five SQUID sets and shows a highly linear dependence: $L_{co} = L_0\ell_1 + L_{end}$. L_{end} is the same for all SQUIDs in each set and is due to small extra contributions to inductance at the shorted end and around the terminals. Experimental values of L_0 are listed in Table II, along with our estimates of λ at 77 K based on these data, using the following procedures.

To estimate $\lambda(77)$, we use `3D-MLSI` to extract L_0 for each style of SQUID. `3D-MLSI` also visualizes current flow, as shown in Fig. 3. Current bunching is evident at the closed end and around the terminals. This adds extra inductance to L_{co}, which, as for the experiment, we eliminated by extracting L_{co} for a range of lengths ℓ_1 and regression to $L_{co}(\ell_1)$. For comparison, we also used `FastHenry`[33] and the program `induct`,[34] derived from work by Chang.[35] Induct derives L_0 directly for infinitely long lines. For `FastHenry`, we extracted the inductance L_{CPS} of a pair of anti-parallel open-circuit lines for a range of lengths ℓ. Again, regression to $L_{CPS}(\ell)$ was done to find L_0, to avoid end effects to do with the point-injection of current into lines of finite width by `FastHenry`. These three extraction tools all include L_{kin}. For all of them, λ is a user-defined parameter, but the form of its temperature dependence is *not*.

Each extractor was run for $100 < \lambda < 500$ nm in 25 nm steps. The resulting $L_0 - \lambda$ data-sets were fitted to a polynomial expression for $\lambda(L_0)$. We then used the experimental value of L_0 to derive our estimate of $\lambda(77)$ for each of the five SQUID designs. Table II brings together these data for all three extraction methods. We have greatest confidence in the values of $\lambda(77)$ using the FEM package `3D-MLSI`, though for extracting L_0 for the CPS structure, both `FastHenry` and induct give similar answers, as Table II confirms.

TABLE II. Measured data and the values deduced for λ. Each of the five sets has four SQUIDs with different values of ℓ_1. $L_{co} = \Phi_0/\delta I$ was measured for each SQUID, and L_0 was derived from the $L_{co}(\ell_1)$ data for each set. λ_{mlsi}, λ_{ind}, and λ_{fh} are from fits to inductance extraction data using `3D-MLSI`, `induct`, and `FastHenry` models, respectively.

Set	SQUID	ℓ_1 (μm)	δI (μA)	L_{CO} (pH)	L_0 (pH/μm)	λ_{mlsi} (nm)	λ_{ind} (nm)	λ_{fh} (nm)
	SQ1	50	31.48	65.69				
S1-A	SQ2	75	21.18	97.64	1.291	402	401	404
	SQ3	100	15.88	130.23				
	SQ4	125	–	–				
	SQ1	20	60.66	34.09				
S2-A	SQ2	34	–	–	1.669	386	385	387
	SQ3	44	27.94	74.01				
	SQ4	50	24.64	83.92				
	SQ1	20	57.66	35.86				
S3-A	SQ2	34	34.48	59.97	1.734	401	399	401
	SQ3	44	26.84	77.04				
	SQ4	50	23.48	88.07				
	SQ1	20	84.00	24.62				
S3-B	SQ2	30	58.34	35.44	1.097	384	370	377
	SQ3	40	44.58	46.38				
	SQ4	50	35.94	57.54				
	SQ1	20	98.68	20.95				
S3-C	SQ2	30	67.16	30.79	0.984	385	359	363
	SQ3	40	50.36	41.06				
	SQ4	50	40.28	51.34				

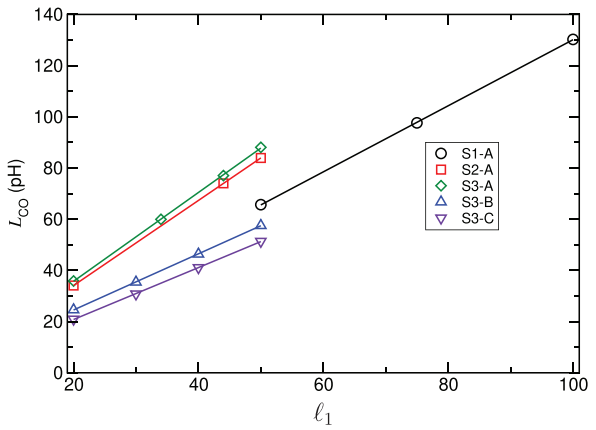

FIG. 2. The measured coupled SQUID inductance L_{co} vs its length ℓ_1 for the five different SQUID sets. Each solid line is a linear fit to the data points and its gradient is L_0.

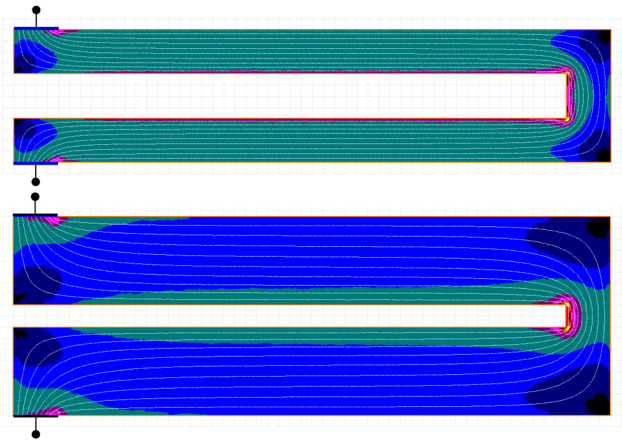

FIG. 3. Layouts and stream function solutions for SQUIDs S1-A (SQ1) and S3-C (SQ4), both with $\ell_1 = 50$ μm, for $\lambda = 400$ nm. Current flows in and out through 4 μm wide terminals marked ●. Colors represent the magnetic field generated, black lowest, red highest, on a normalized scale of 0 to 1.0.

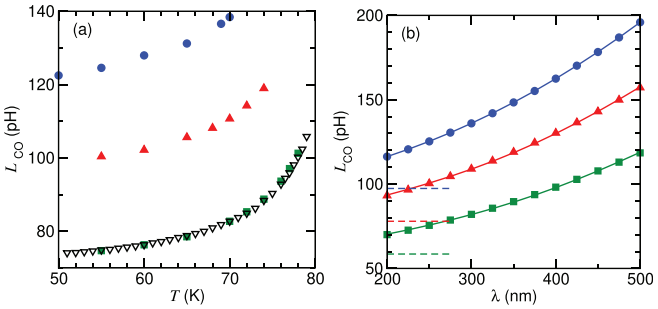

FIG. 4. (a) Measured inductance L_{co} as a function of temperature T for three SQUIDs from set S1-A ● SQ4; ▲ SQ3; ▽ and ■ SQ2. Devices SQ4 and SQ3 had smaller flux modulation, owing to their higher L_{sq}, which limited measurements of L_{co} to less than 70 and 74 K, respectively. The two data-sets for SQ2 were recorded on different occasions. (b) L_{co} extracted by `3D-MLSI`, varying λ, for the same set of SQUIDs. Solid lines are cubic fits. Dashed lines indicate values of L_{ext} for each SQUID.

In the second stage of our work, we used a cryocooler to measure three SQUIDs, one by one, from set S1-A, to get $L_{co}(T)$ for each, as shown in Fig. 4(a). The temperature was measured by a PT-111 RTD sensor, mounted on the copper block carrying the substrate, 6 mm from its edge. A Lakeshore 335 controller with a 50 Ω heater regulated the temperature to $\approx \pm 0.1$ K.

We then used `3D-MLSI` with structures like those in Fig. 3 to extract L_{co}, for $200 < \lambda < 500$ nm, and these data were fitted to functions for $L_{co}(\lambda)$, as shown in Fig. 4(b). We then merged $L_{co}(\lambda)$ with the experimental values of $L_{co}(T)$ for the three SQUIDs to generate our consolidated result for $\lambda(T)$, as shown in Fig. 5. It is clear that our data derived from four separate measurements on three different SQUIDs have the same temperature dependence, which we believe validates our measurement of L_{co}(T) and our analysis using `3D-MLSI`. This is the only extraction package that can be used, as it will correctly include the extra temperature-dependent inductance associated with current flow near the terminals and around the shorted end, as is evident in Fig. 3. Neither `FastHenry`, nor induct nor CPS formulas can include these effects. The dashed lines in Fig. 4(b) are L_{ext} values for each SQUID, found from `3D-MLSI` by setting $\lambda = 0$, which makes $L_{kin} = L_m = 0$. This clearly shows the significant contribution from L_{kin} to the total inductance in this temperature range.

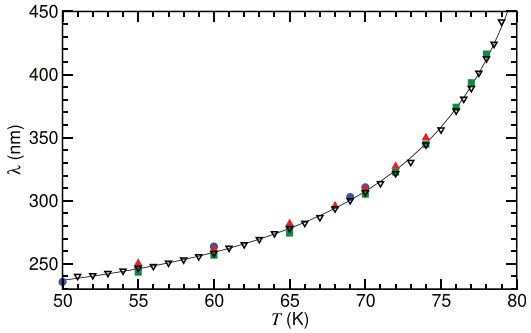

FIG. 5. $\lambda(T)$ derived from the data shown in Figs. 4(a) and 4(b) for the same three SQUIDs. Data markers are the same as those in Fig. 4. The solid line is a fit to (1) with $T_c = 85.9$ K.

We made a non-linear least squares fit to these data, assuming that $\lambda(T)$ has this general form,

$$\lambda(T) = \lambda(0)\left[1 - (T/T_c)^P\right]^{-n}. \quad (1)$$

The solid line in Fig. 5 has $\lambda(0)$ and P as fitting parameters, with fixed $n = 0.5$ and $T_c = 85.9$ K, the measured value. This gives $\lambda(0) = 217$ nm and $P = 3.36$.

The form of (1) is based on the two-fluid Gorter-Casimir *ad hoc* expression for the super-electron density n_s and the London expression for $\lambda(n_s)$, which give $P = 4$ and $n = 0.5$ for low-temperature superconductors. There is no underlying microscopic reason to expect specific values of P or indeed n for our HTS thin films. Our value of P exceeds the 1.94–2.45 range found some while ago by Il'ichev *et al.*[36] Others generally found $P \approx 2$.[17,21,37–39] Our value of 217 nm for $\lambda(0)$ is within the accepted range of other measurements, for example,[37,40,41] for transport in the *a-b* plane of high-quality YBCO thin films.

To conclude our work, we extended our inductance extraction methods to compare the measured and simulated effective areas of a set of our directly coupled magnetometers (DCM's). Figure 6 shows one of the DCM's.

All the DCM's have the same size of split-washer pickup loop, directly coupled to two SQUIDs in series that can be biased individually. These SQUIDs have the same geometry as those in Fig. 1 and Table I but have different dimensions and are identified in Table III as types D, E, and F. DCMs differ one from another by the types of SQUIDs they contain, which can be any two from D, E, or F. In total, 15 DCMs were measured, six using SQUID type D, five type E, and four type F. The DCMs are all made from YBCO films 220 nm thick and were measured at 77 K, so for inductance extraction, we used $\lambda = 402$ nm, as given in Table II.

To simulate measurement of the effective area A_{eff}^{w} of the washer, we added an extra conductor to the `3D-MLSI` model, designed to generate a reasonably uniform field B_z through the x–y plane of the entire device.[42] If a current I in this induces a flux Φ in the washer, then

$$A_{eff}^{w} = \Phi/B_z = (M_f I)/B_z = M_f/\alpha, \quad (2)$$

where M_f is the mutual inductance between the field generator and washer, as simulated by `3D-MLSI`, and $B_z = \alpha I$, with α found by Biot–Savart. We used a pair of in-plane parallel tracks, far away from either side of the device, which generate an acceptably uniform B_z. The

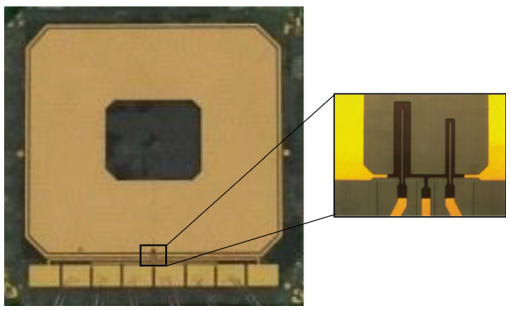

FIG. 6. A directly coupled magnetometer with a washer-style pickup loop on a 1 cm^2 substrate. The overall size of the washer is 8.2×7.5 mm^2, the hole is 3.2×2.7 mm^2, and the slit in the washer is 6 μm wide. Each DCM contains two SQUIDs with L_{co} in series, as shown in the inset, types D and E in this example.

TABLE III. Data and effective areas for the three types of DCM. All have the same washer dimensions, but use SQUIDs that differ in the values of ℓ_1. All have uncoupled lengths $\ell_0 = 8\,\mu$m. In this Table, inductances are in pH, lengths in μm, and areas in mm^2. The error is the fractional difference between measured and simulated data.

SQUID type	ℓ_1	s	w_1	L_{co}	L_w/L_{co}	L_{sq}	A^m_{eff} (model)	A^m_{eff} (meas.)	Error %
D	76	2	8	67.35	79.3	85.62	0.268	0.254	5.5
E	61	2	4	71.59	74.6	89.07	0.285	0.272	4.8
F	72	4	4	94.31	56.6	117.2	0.376	0.350	7.4

same principle was used to find A^{sq}_{eff} for each of the three SQUID types used in the magnetometers.

Owing to the very different scales of the washer and the SQUID (as Fig. 6 shows), their `3D-MLSI` models need different FEM meshing arrangements and so we ran models for the washer and the SQUID separately. We found the washer self-inductance $L_w = 5,342$ pH and A^w_{eff}=21.29 mm^2. The SQUIDs had A^{sq}_{eff} in the range 398 to 720 μm^2. We also extracted values of the coupled inductance L_{co} for each SQUID type. The expected effective area of the magnetometer can then be calculated from the simulation data

$$A^m_{eff} = (L_{co}/L_w)A^w_{eff} + A^{sq}_{eff} \approx (L_{co}/L_w)A^w_{eff}. \quad (3)$$

A^{sq}_{eff} is negligible, compared to A^m_{eff}, and we also neglect mutual inductance between the washer and SQUID.

Experimentally, A^m_{eff} was found by applying a known magnetic field with a calibrated long solenoid and measuring over a minimum of $10\Phi_0$ with the flux-locked loop (FLL) unlocked. All measurements were made inside three layers of mu-metal shielding using Magnicon SEL FLL electronics.[43]

Table III summarizes the results of our simulations and the experimental values of A^m_{eff}. The measured A^m_{eff} is averaged for each set of DCMs operating with the same type of SQUID. We have also included simulated values of L_{sq}, the total SQUID inductance, which are considerably higher than L_{co}, due to the extra structure across the step-edge junctions with 2 μm wide tracks that close the SQUID loop.

In summary, by direct inductance measurements on twenty SQUIDs and inductance extraction by `3D-MLSI`, we find that $\lambda(77)$ is in the range 384 to 402 nm for 220 and 133 nm films, with a mean of 391 nm. We find that $\lambda(77)$ is broadly independent of film thickness and film batch, which we believe confirms the high quality of all our films. There are insufficient data to identify any clear dependence on T_c. In general, there is good agreement for each SQUID set between λ_{mlsi}, λ_{ind}, and λ_{fh}, the values obtained at 77 K using `3D-MLSI`, induct, and `FastHenry`. From SQUIDs with 220 nm thick films measured in a cryo-cooler, we found a close fit to (1) for $\lambda(T)$ between 50 and 79 K. We view (1) as an empirical design aid for calculating the inductance of SQUID and SQIF loops to give optimum performance at any temperature. We used our inductance extraction methods to predict the effective areas of a directly coupled magnetometers, which agree with the experimental value to better than 7.4%.

DATA AVAILABILITY

The data that support the findings of this study are available from the corresponding authors upon reasonable request.

REFERENCES

[1]S. T. Keenan, J. Du, E. E. Mitchell, S. K. H. Lam, J. C. Macfarlane, C. J. Lewis, K. E. Leslie, and C. P. Foley, IEICE Trans. Electron. **E96.C**, 298 (2013).
[2]R. L. Fagaly, *Superconducting Quantum Interference Devices (SQUIDs)* (John Wiley & Sons, Inc., 2016), pp. 1–15.
[3]R. Stolz, M. Schmelz, V. Zakosarenko, C. P. Foley, K. Tanabe, X. Xie, and R. Fagaly, Supercond. Sci. Technol. **34**, 033001 (2021).
[4]J. B. Lee, D. L. Dart, R. J. Turner, M. A. Downey, A. Maddever, G. Panjkovic, C. P. Foley, K. E. Leslie, R. Binks, C. Lewis, and W. Murray, Geophysics **67**, 468 (2002).
[5]K. E. Leslie, R. A. Binks, S. K. H. Lam, P. A. Sullivan, D. L. Tilbrook, R. G. Thorn, and C. P. Foley, Leading Edge **27**, 70 (2008).
[6]S. T. Keenan, J. A. Young, C. P. Foley, and J. Du, Supercond. Sci. Technol. **23**, 025029 (2010).
[7]S. Linzen, V. Schultze, A. Chwala, T. Schüler, M. Schulz, R. Stolz, and H.-G. Meyer, *Quantum Detection Meets Archaeology—Magnetic Prospection with SQUIDs, Highly Sensitive and Fast* (Springer, Berlin/Heidelberg, 2009).
[8]H.-J. Krause, M. Mück, and S. Tanaka, in *Applied Superconductivity: Handbook on Devices and Applications*, edited by P. Seidel (Wiley-VCH Verlag GmbH, Weinheim, 2015), pp. 977–992.
[9]E. E. Mitchell, K. E. Hannam, J. Lazar, K. E. Leslie, C. J. Lewis, A. Grancea, S. T. Keenan, S. K. H. Lam, and C. P. Foley, Supercond. Sci. Technol. **29**, 06LT01 (2016).
[10]J. Oppenländer, C. Häussler, A. Friesch, J. Tomes, P. Caputo, T. Träuble, and N. Schopohl, IEEE Trans. Appl. Supercond. **15**, 936 (2005).
[11]S. K. H. Lam, R. Cantor, J. Lazar, K. E. Leslie, J. Du, S. T. Keenan, and C. P. Foley, J. Appl. Phys. **113**, 123905 (2013).
[12]A. T. Fiory, A. F. Hebard, P. M. Mankiewich, and R. E. Howard, Appl. Phys. Lett. **52**, 2165 (1988).
[13]J. H. Claassen, M. L. Wilson, J. M. Byers, and S. Adrian, J. Appl. Phys. **82**, 3028 (1997).
[14]R. F. Wang, S. P. Zhao, G. H. Chen, and Q. S. Yang, Appl. Phys. Lett. **75**, 3865 (1999).
[15]X. He, A. Gozar, R. Sundling, and I. Bozovic, Rev. Sci. Instrum. **87**, 113903 (2016).
[16]R. Prozorov and R. W. Giannetta, Supercond. Sci. Technol. **19**, R41 (2006).
[17]M. G. Forrester, A. Davidson, J. Talvacchio, J. R. Gavaler, and J. X. Przybysz, Appl. Phys. Lett. **65**, 1835 (1994).
[18]D. Grundler, B. David, and O. Doessel, J. Appl. Phys. **77**, 5273 (1995).
[19]H. Fuke, K. Saitoh, T. Utagawa, and Y. Enomoto, Jpn. J. Appl. Phys. **35**, L1582 (1996).
[20]E. E. Mitchell, D. L. Tilbrook, C. P. Foley, and J. C. MacFarlane, Appl. Phys. Lett. **81**, 1282 (2002).
[21]H. Li, E. Y. Cho, H. Cai, Y. Wang, S. J. McCoy, and S. A. Cybart, IEEE Trans. Appl. Supercond. **29**, 1600404 (2019).
[22]S. Ruffieux, A. Kalaboukhov, M. Xie, M. Chukharkin, C. Pfeiffer, S. Sepehri, J. F. Schneiderman, and D. Winkler, Supercond. Sci. Technol. **33**, 025007 (2020).
[23]S. Ruffieux, N. Lindvall, A. Kalaboukhov, J. F. Schneiderman, and D. Winkler, "Optimization of single layer high-T_c SQUID magnetometers for low noise," in ASC 2020 (unpublished).
[24]Y. Shimazu and T. Yokoyama, Physica C **412–414**, 1451 (2004).
[25]J. Y. Lee and T. R. Lemberger, Appl. Phys. Lett. **62**, 2419 (1993).
[26]K. Yoshida, M. S. Hossain, T. Kisu, K. Enpuku, and K. Yamafuji, Jpn. J. Appl. Phys., Part 1 **31**, 3844 (1992).
[27]M. M. Khapaev, A. Y. Kidiyarova-Shevchenko, P. Magnelind, and M. Y. Kupriyanov, IEEE Trans. Appl. Supercond. **11**, 1090 (2001).
[28]M. M. Khapaev and M. Y. Kupriyanov, Supercond. Sci. Technol. **28**, 055013 (2015).
[29]C. Foley, E. Mitchell, S. Lam, B. Sankrithyan, Y. Wilson, D. Tilbrook, and S. Morris, IEEE Trans. Appl. Supercond. **9**, 4281 (1999).
[30]E. E. Mitchell and C. P. Foley, Supercond. Sci. Technol. **23**, 065007 (2010).
[31]See http://ceraco.de for "Ceraco Ceramic Coating GmbH," Ismaning, Germany.
[32]See http://starcryo.com for "STAR Cryoelectronics," Santa Fe, USA.
[33]M. Kamon, M. J. Tsuk, and J. K. White, IEEE Trans. Microwave Theory Tech. **42**, 1750 (1994).
[34]See http://www.wrcad.com for "IC Design Software for Linux, OS X and Windows," Whiteley Research, Inc.

[35]W. H. Chang, IEEE Trans. Magn. **17**, 764 (1981).
[36]E. Il'ichev, L. Dörrer, F. Schmidl, V. Zakosarenko, P. Seidel, and G. Hildebrandt, Appl. Phys. Lett. **68**, 708 (1996).
[37]D.-X. Chen, C. Navau, N. Del-Valle, and A. Sanchez, Physica C **500**, 9 (2014).
[38]S. D. Brorson, R. Buhleier, J. O. White, I. E. Trofimov, H.-U. Habermeier, and J. Kuhl, Phys. Rev. B **49**, 6185 (1994).
[39]M. Prohammer and J. P. Carbotte, Phys. Rev. B **43**, 5370 (1991).
[40]A. G. Zaitsev, R. Schneider, G. Linker, F. Ratzel, R. Smithey, P. Schweiss, J. Geerk, R. Schwab, and R. Heidinger, Rev. Sci. Instrum. **73**, 335 (2002).
[41]E. Farber, S. Djordjevic, N. Bontemps, O. Durand, J. Contour, and G. Deutscher, J. Low Temp. Phys. **117**, 515 (1999).
[42]G. Gerra, "Electromagnetic modelling of superconducting sensor designs," Master's thesis (University of Cambridge, 2003).
[43]See http://magnicon.com for "Physical research and instrumentation," Magnicon GmbH, Hamburg, Germany.